Simulation software for transition-edge sensor performance prediction

Simulation software for transition-edge sensor performance prediction

H. Garrone, C. Pepe, A. Reineri, E. Monticone, R. Filippo, and M. Rajteri

***Abstract*—Transition-edge sensors (TES) are outstanding calorimeters based on the steep superconductive transition of a metallic film. Among other photon detectors, they are renowned for the fine energy resolution, the photon-number resolving (PNR) capability and an extremely low dark count rate. Due to the broad detection spectrum, from gamma-ray to visible and submillimetre wavelengths, TESs are highly sought-after in a great variety of fields, such as X-ray detection and quantum technologies. Each of these fields demands a step forward in TESs performance with regards to the recovery time and energy resolution. Here we present a program, primarily capable of predicting the performance of TESs. Using established theoretical and empirical methods we developed a software that allows the users to choose active area, thickness, and material composition of a TES and to calculate its performance. Furthermore, the software can simulate TES properties at different working points. The aim of the software is to minimize the production cost and speed up the overall process for the creation of new devices with improved performance.**

***Index Terms*—Transition-edge sensors, low temperature detector, simulation software.**

I. Introduction

THE SIMULATION of sensors performance is a key aspect for the design of any photon and particle detection experiment. Transition-edge sensors (TESs) are microcalorimeters among the best candidates able to achieve excellent energy resolution together with photon number resolving capability [1],[2],[3]. An energy resolution of 0.11 eV was already reached for infrared photons [4], however, some applications require this outcome to be further improved, for instance the PTOLEMY project requires a particle detector with energy resolution better than 0.05 eV [5]. TESs exploit the steep resistance transition of a metallic film from superconductive to normal state; when a photon is absorbed, it releases its energy causing a temperature rise corresponding to a high resistance increment. The energy resolution is directly dependent on the critical temperature (T_C) of the film and the volume of the device. Furthermore, it improves by increasing the steepness of the transition. The T_C of a TES depends on the T_C of the chosen superconductor and possibly on the proximity effect due to the presence of an additional normal layer [6],[7].

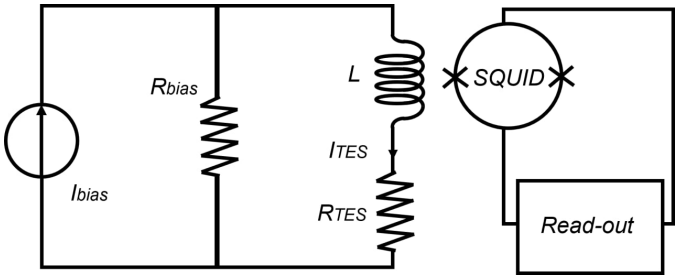

Fig. 1. Schematic of the device bias circuit. The TES is operated in voltage bias mode, a dc-SQUID is used as transimpedance amplifier.

The prediction of TESs performance relies on well known theoretical and empirical models summarised by Irwin and Hilton in [8] as a development from a more general theory for bolometers noise presented in [9]. In section II, the Irwin-Hilton model, the proximity effect [10], the two-fluid and weak-link models [11–14] are summarised. Section III describes how these models are combined into a program that allows the users to simulate and predict TESs performance. In section IV simulated results are compared to literature results and a case study applied to the PTOLEMY project requirement is presented.

II. Physical Model

A. Irwin-Hilton configuration

Let a TES be part of an electro-thermal circuit (Fig. 1) and be operated in voltage bias mode; the physics of the system is summarised by the following equation taken from [8]. The current circulating in the TES is:

$$I_{\mathrm{TES}} = \frac{R_{\mathrm{shunt}}}{R_{\mathrm{shunt}} + R_{\mathrm{par}} + R_{\mathrm{TES}}} I_{\mathrm{bias}} \tag{1}$$

where R_{TES} is the resistance of the TES, R_{par} is the parasitic resistance of the circuit in the TES branch and R_{shunt} is a shunt resistance in parallel to the TES. I_{bias} is the bias current of the overall circuit.

In stationary thermal conditions the rate of heat flow from the TES to the thermal bath is equal to the power due to the Joule effect, hence I_{TES} is equal to:

$$I_{\mathrm{TES}} = \sqrt{\frac{k(T_0^n - T_{\mathrm{bath}}^n)}{R_{\mathrm{TES}}}} \tag{2}$$

Manuscript receipt and acceptance dates will be inserted here.
(Corresponding author: Carlo Pepe.)

C. Pepe is with the Politecnico di Torino, Corso Duca degli Abruzzi 24, 10129 Torino, Italy and also with Istituto Nazionale di Ricerca Metrologica (e-mail: carlo.pepe@polito.it).

H. Garrone and A. Reineri are with the Physics department Università di Torino, Via Pietro Giuria 1, 10125 Torino, Italy (e-mail: hobey.garrone@edu.unito.it, alessandro.reiner@edu.unito.it).

E. Monticone, R. Filippo and M. Rajteri are with the Istituto Nazionale di Ricerca Metrologica , Strada delle Cacce, 91 10135 Torino, Italy (e-mail: e.monticone@inrim.it, r.filippo@inrim.it, m.rajteri@inrim.it).

with T_0 the TES temperature in the stationary working condition, T_{bath} the temperature of the thermal bath, n the thermal conductance exponent and $k = \sum_{i=0}^{N} \Lambda_i \cdot V_i$. Where V_i volume and Λ_i is the electron phonon coupling constant of the ith layer of N layers [15]. The low frequency loop gain of the circuit in stationary state $\mathscr{L}$ and the characteristic time τ of the circuit are defined as:

$$\begin{cases} \mathscr{L} \equiv \dfrac{I_{\text{TES}}^2 R_{\text{TES}} \cdot \alpha_{\text{I}}}{G\, T_0} \\ \tau \equiv \dfrac{C}{G} \end{cases} \tag{3}$$

where C and G are the TES thermal capacitance and conductance, respectively, and $\alpha_{\text{I}} = \left.\frac{\partial ln(R)}{\partial ln(T)}\right|_{I_{\text{TES}}}$ is the logarithmic temperature sensitivity. The photons absorbed by the TES generate electrical signals that are readout through an inductance L coupled to a dc-SQUID used as transimpedance amplifier. For small values of L (see [8]), the electrical time constant τ_{el} and the effective thermal time constant τ_{eff} are:

$$\begin{cases} \tau_{\text{el}} = \dfrac{L}{R_{\text{L}} + R_{\text{TES}}(1+\beta_{\text{I}})} \\ \tau_{\text{eff}} = \tau \dfrac{1 + \beta_{\text{I}} + \frac{R_{\text{L}}}{R_{\text{TES}}}}{1 + \beta_{\text{I}} + \frac{R_{\text{L}}}{R_{\text{TES}}} + \left(1 - \frac{R_{\text{L}}}{R_{\text{TES}}}\right)\mathscr{L}} \end{cases} \tag{4}$$

where $\beta_{\text{I}} = \left.\frac{\partial ln(R)}{\partial ln(I)}\right|_{T_0}$ and $R_{\text{L}} = R_{\text{shunt}} + R_{\text{par}}$.
A TES operating in stable conditions can have an overdamped or underdamped response. The stability constraint in the first case is:

$$R_{\text{TES}} > \frac{\mathscr{L} - 1}{\mathscr{L} + 1 + \beta_{\text{I}}} R_{\text{L}} \tag{5}$$

whereas in the underdamped response the constraints are:

$$\mathscr{L} \leq 1 \quad or \quad \begin{cases} \mathscr{L} > 1 \\ L < \frac{\tau}{\mathscr{L}-1}[R_{\text{L}} + R_{\text{TES}}(1+\beta_{\text{I}})] \end{cases} \tag{6}$$

The energy resolution (ΔE_{FWHM}) of the TES is influenced by the Johnson noise voltage of the TES ($S_{V_{\text{TES}}}$) and of the load resistor ($S_{V_{\text{th}}}$), the thermal fluctuation noise ($S_{P_{\text{TFN}}}$) and SQUID amplifier noise (S_{SQUID}). ΔE_{FWHM} is calculated as:

$$\begin{aligned} &\Delta E_{\text{FWHM}} = 2\sqrt{2\ln 2} \times \\ &\times \left\{ \frac{\tau I_0^2}{\mathscr{L}^2} \left[\left(\frac{\mathscr{L}^2}{I_0^2} S_{P_{\text{TFN}}} + S_{V_{\text{TES}}} + (\mathscr{L}-1)^2 S_{V_{\text{th}}} \right) \times \right. \right. \\ &\times \left(S_{V_{\text{TES}}} + S_{V_{\text{th}}} \right) + \\ &\left. \left. + \left(\mathscr{L}(R_{\text{TES}} - R_{\text{L}}) S_{\text{SQUID}} \right)^2 \right]^{\frac{1}{2}} \right\}^{\frac{1}{2}}. \end{aligned} \tag{7}$$

with $S_{V_{\text{th}}} = 4k_{\text{B}}T_0R_{\text{L}}$, $S_{V_{\text{TES}}} = 4k_{\text{B}}T_0R_{\text{TES}}\chi(I)$ and $S_{P_{\text{TFN}}} = 4k_{\text{B}}T_0^2G \cdot F(T_0, T_{\text{bath}})$. The term $\chi(I)$ is introduced to take into account the resistor non-linear current dependency and $F(T_0, T_{\text{bath}})$ is the correction due to non-linear dependency of G from temperatures, (more details in [16]). A simplified version of this formula is:

$$\Delta E = 2\sqrt{2\ln 2}\sqrt{4k_{\text{B}}T_0^2 \frac{C}{\alpha_{\text{I}}}\sqrt{\frac{n}{2}}} \tag{8}$$

To be thorough, we report the formulas that were used to compute the thermal capacitance, the thermal conductance and the TES saturation energy.
Thermal capacitance [17]:

$$C = \left(2.43 \cdot \gamma T_0 + \zeta T_0^3\right) V \tag{9}$$

where V is the volume, γ is the Sommerfeld constant and $\zeta = \frac{12.3 \cdot \pi^4 R}{5 \cdot T_{\text{D}}^3} \frac{D}{W}$. W is the atomic weight, D is the volumic density, T_{D} is the Debye temperature, and R the gas constant.
Thermal conductance [17]:

$$G = n k T_0^{n-1}. \tag{10}$$

Saturation energy E_{sat} is [18]:

$$E_{\text{sat}} = C\Delta T \approx \frac{C T_0}{\alpha_{\text{I}}}. \tag{11}$$

B. Proximity effect

A bilayer, made up of a superconductor layer and a normal metal layer, has a critical temperature T_{C} lower than the intrinsic critical temperature T_{C0} of the superconductor due to the proximity effect. Assuming the layers thicknesses to be comparable with the coherence length of the materials, one can express the overall T_{C} of the bilayer as follows [10]:

$$T_{\text{C}} = T_{\text{C0}} \left[\frac{d_{\text{s}}}{d_0} \frac{1}{1.13\left(1 + \frac{1}{a}\right)t} \right]^a \tag{12}$$

where t is the transmission coefficient, $\frac{1}{d_0} = \frac{\pi}{2} k_{\text{B}} T_{C0} n_{\text{s}} \lambda_{\text{F}}^2$, with λ_{F} the Fermi wavelength, and the exponent a equal to:

$$a = \frac{d_{\text{n}} n_{\text{n}}}{d_{\text{s}} n_{\text{s}}}. \tag{13}$$

The terms d_{n} and d_{s} are the thicknesses and n_{n}, n_{s} are the electron state densities of normal and superconductive layers, respectively. For normal layer thickness greater than 50 nm we used the transmission coefficient modified formula [10]:

$$\frac{1}{t} \rightarrow \frac{1}{t} + \frac{1}{3}\frac{d_{\text{n}}}{\sigma_{\text{n}}} \frac{2G_{\text{k}}}{\left(\frac{\lambda_{\text{F}}}{2}\right)^2} \tag{14}$$

where $G_{\text{k}} = \frac{e^2}{h}$ and σ_{n} stands for the normal layer conductivity. e is the electron charge and h is the Planck constant.

C. Transition models

The parameters α_I and β_I can be extrapolated through models that describe the resistance dependency with respect to the current and the temperature. In [11], Ullom *et al.* summarise the two most commonly used models. One is the two-fluid model and the other is the weak-link model. In both these models the resistance is expressed as a function of the TES current I_{TES} and of the critical current I_C. I_C is a function of the TES temperature T_0 and the critical temperature T_C.

1) Two-fluid model: In the two-fluid model the critical current is:

$$I_C(T_0) = I_{C0}\Big(1-\frac{T_0}{T_C}\Big)^{\frac{3}{2}} \tag{15}$$

whereas the resistance expression is:

$$R(I_{TES},T_0) = c_R R_N\Big(1-c_I\frac{I_C(T_0)}{I_{TES}}\Big) \tag{16}$$

where $I_{C0}=I_C(0)$, R_N is the normal resistance and c_R, c_I are phenomenological parameters describing the normal and superconductive carriers channels. Thus the parameters β_I and α_I are obtained as follows [19]:

$$\beta_I = c_R\frac{R_N}{R_{TES}}-1 \tag{17}$$

$$\alpha_I = \frac{3}{2}\left[\beta_I^{\frac{1}{3}}\left(\frac{(\beta_I+1)c_I I_{C0}}{I_{TES}}\right)^{\frac{2}{3}}-\beta_I\right]. \tag{18}$$

2) Weak-link model: With the assumption that the distance between the leads is comparable to the effective coherent length of the superconductor, the resistance is given by [11]:

$$R(I_{TES},T_0) = R_N\left[1-\left(\frac{I_C(T_0)}{I_{TES}}\right)^2\right]^{\frac{1}{2}}. \tag{19}$$

On the other hand, I_C shows an exponential decrease with respect to the length. A compact form of the formula is [11]:

$$I_C(T_0,l) = I_{C0}V^*\frac{l}{\xi^*}\exp\left(-\frac{l}{\xi^*}\right) \tag{20}$$

with l being the weak-link length. ξ^* is the effective decay length for arbitrary T_{Ci} calculated in the framework of the Usadel equations by Kupriyanov *et al.* [20] as:

$$\xi^*(T_0) = \xi_N\sqrt{\frac{T_{CL}}{T_0}\Big[1+\frac{\pi^2}{4}\ln^{-1}\Big(\frac{T_0}{T_{Ci}}\Big)\Big]} \tag{21}$$

where T_{Ci} is the intrinsic critical temperature of the weak-link, T_{CL} is the critical temperature of the leads and ξ_N is the intrinsic coherent length of the material at $T>T_{Ci}$.

Whereas V^* has the analytic expression:

$$V^*(T_0) = \frac{32\cdot T_0\cdot\Delta^2}{T_{CL}\Big[\mathscr{E}+\Delta^*+\sqrt{2\Delta^*(\mathscr{E}+\Delta^*)}\Big]^2} \tag{22}$$

with $\mathscr{E}=\pi k_B T_0$, $\Delta^*(T_0)=\sqrt{(\pi k_B T_0)^2+\Delta^2}$ and the *gap* in the isotropic superconductive electrodes Δ is well approximated as:

$$\Delta = 1.76\cdot k_B T_0\tanh\left[\frac{\pi}{1.76}\sqrt{\Big(\frac{T_{CL}}{T_0}-1\Big)}\right] \tag{23}$$

Then the parameter α_I is finally obtained deriving the critical current with respect to the temperature, whereas β_I has an expression similar to the one derived in the two-fluid model:

$$\alpha_I = -\Big(\frac{R_N}{R_{TES}}\frac{I_C(T_0)}{I_{TES}}\Big)^2\frac{\partial\ln(I_C)}{\partial\ln(T)}\Big|_{T_0} \tag{24}$$

$$\beta_I = \Big(\frac{R_N}{R_{TES}}\Big)^2-1 \tag{25}$$

In both these models, an approximation of I_{C0} is given by [21]:

$$I_{C0} = 3.52\sqrt{\frac{k_B C}{\hbar R_N}}T_C \tag{26}$$

3) Critical exponent model: Besides the previous two models, the resistance can be expressed in the form of critical exponent formulation as:

$$R = \frac{R_N}{1+e^{4.4\cdot\frac{(T_C-T)}{\Delta T}}} \tag{27}$$

where $\Delta T = T(R_{TES}=90\,\%\cdot R_N)-T(R_{TES}=10\,\%\cdot R_N)$. The value of α_I is obtained through its definition with this expression of the resistance.

III. Software

Here we present a program which exploits the models discussed in the previous section. The program is based on *G Web Development Software*, a programming environment developed by *National Instrument*. The ansatzes for this program are: rectangular TESs and $T_0=T_C$. The flowchart diagram of the program is shown in Fig. 2.

Firstly the user chooses the materials, enters the active area parameters and the thickness of each of the selected layers. The program has a precompiled list of common used materials in literature, with their related parameters, however the user is allowed to modify them.

The second step is to manually enter the value of T_C, or allow the program to automatically calculate it, using the proximity effect model. In the latter scenario the user must choose two layers only, and enter the value of t.

The third step is the choice of the model. The first option is the manual mode, the program requires to enter the values of α_I and β_I, or enable the critical exponent calculation and enter the value of β_I and ΔT. Instead, if the weak-link model option is selected, the user must enter the values of the following parameters: I_{C0}, ξ_N, T_{Ci} and T_{CL}. In the third option, I_{C0}, c_R and c_I are required as inputs to exploit the two-fluid model. The parameter I_{C0} could be entered by the user or automatically computed by (26). After the determination of α_I and β_I, the fourth step consists in the choice between calculating ΔE with the complete formula

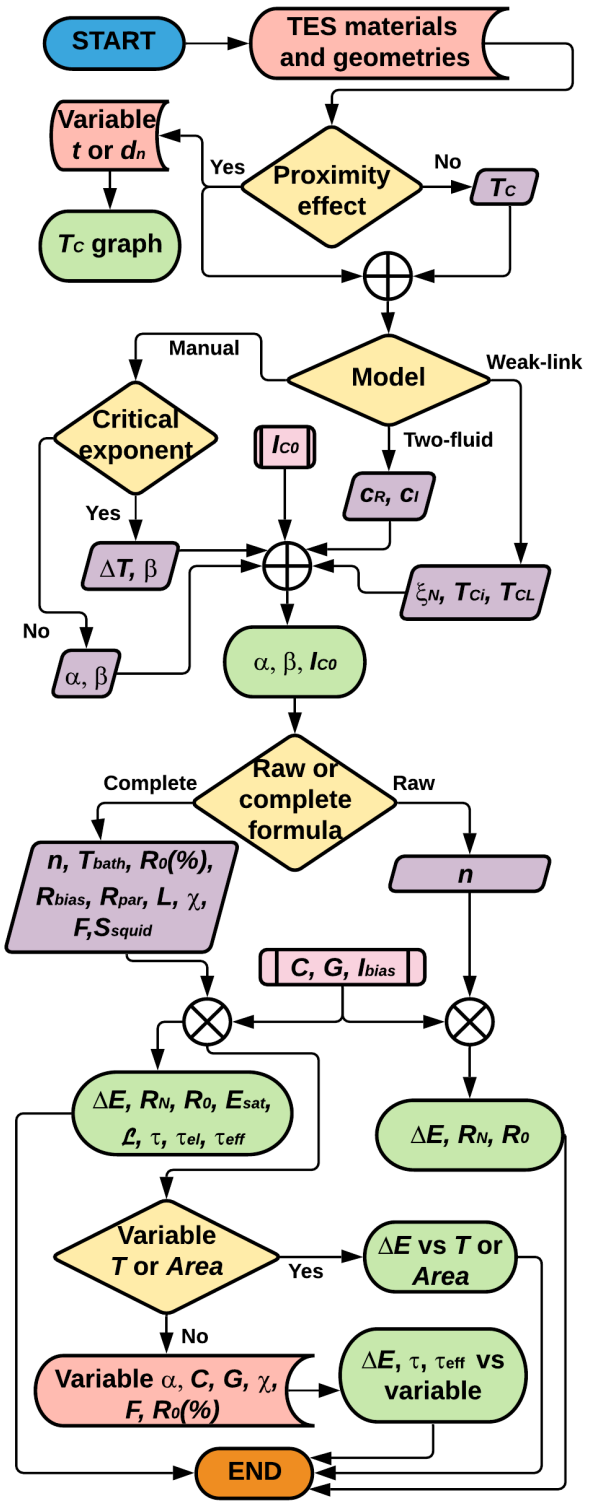

Fig. 2. Flowchart of the program. Oval is used as *terminal*, diamond as *decision* , half-cylinder as *stored data*, parallelogram as *input*, rectangular as *sub-routine*, vertical cross as *or* and diagonal cross as *and*.

(7) and a simplified one (8). If the complete formula is selected, the following inputs are required: n, L, T_{bath}, R_{shunt}, R_{par}, $R_{\mathrm{TES}}(\%)$ (R_{TES} as a percentage of R_{N}) to characterize the electro-thermal circuit and $F(T_0, T_{\mathrm{bath}})$, $\chi(I)$, S_{SQUID}. It is possible to enable the manual insertion of the values of C and G and optionally insert a value for I_{BIAS}, which leads to the computation of I_{TES} through (1) instead of (2). In addition to ΔE, the standard outputs of the simulation are: R_{N}, R_{TES}, I_{TES}, C, G, E_{sat}, $\mathscr{L}$, τ, τ_{el}, τ_{eff} and two boolean indicators for the stability conditions. Moreover, the tool allows to simulate many curves inserting, as inputs, a start value, an end value and a step value.

As an example, if the proximity effect is enabled, the graphs of T_{C} vs. t, d_{n} or d_{s} can be generated. It is also possible to select, as independent variable in the graph, one from S_{Area}, T_{C}, $R_{\mathrm{TES}}(\%)$, R_{shunt}, R_{par}, n, L, I_{BIAS}, C, G, α_{I}, $F(T_0, T_{\mathrm{bath}})$, χ, d_{s}, d_{n}, t, the TES length or the TES width, while, the dependent variable could be one from: ΔE_{FWHM}, E_{sat}, $\mathscr{L}$, τ_{el}, τ_{eff}, C, G, T_{C}, α_{I} and β_{I}.

Therefore, this program not only computes the energy resolution or the other important TESs features, but it also simulates their trends taking into account every dependency. For example, lets consider that T_{C}, α_{I} and β_{I} are calculated from one of the described model and that the user wants to study the trend of ΔE_{FWHM} versus d_{s}. Therefore, this program computes, for all the values of the thickness, the correspondent values of T_{C}, C and G. Also R_{N} is evaluated for each thickness and consequently R_{TES} and I_{TES}. Then I_{C0} and hence α_{I} are computed considering the variation of d_{s}. Finally, the trend of ΔE_{FWHM} versus thickness is obtained considering all the dependencies.

IV. Comparison and Results

A. Comparison between simulated and measured results

In Table I, the measured values of C, G, τ_{eff} and ΔE_{FWHM} are compared to the ones computed by our software for three TESs. The aim of this comparison is to verify the trustworthiness of the software. The comparison is performed for the TESs described in [4], [21–24] from which a rich set of parameters and results is available. TES1,TES2, TES4 and TES5 are TESs characterized for application in the optical range (eV), whereas TES3 was used in the detection of x-rays (keV). The relative deviation between simulated and measured results of τ_{eff} is less than 16 % for the five cases. While energy resolutions can be computed exactly for TES1, TES2, TES4 and TES5 assuming $\chi(I)$ in a range from 1 to 15. In case of TES3 the thermal capacitance was used as input in order to take into account also for the presence of the absorber. For TES3, the excess noise is evaluated as $\chi(I) = (1+2\beta_{\mathrm{I}})(1+M^2) = 66$, considering $M^2 \sim 10$ at $R_{\mathrm{TES}} = 30$ % and $\beta_{\mathrm{I}} = 2.5$ as reported in [23]. With this value our software compute $\Delta E_{\mathrm{FWHM}} = 2.3$ eV, that corresponds to a relative deviation of 8 %.

B. Simulation for PTOLEMY project

To achieve the target of 0.05 eV energy resolution required in the PTOLEMY project we are developing thin

TABLE I
COMPARISON TABLE

	TES1		TES2		TES3		TES4		TES5	
Inputs										
Reference	[4]		[22]		[23]		[21] .		[24]	
Model in the simulation	manual		two-fluids		manual		two-fluids		two-fluids	
Materials	Ti/Au	-	Ti/Au	-	Ti/Au	-	Ti	-	Ti/Au	-
S_{Area} (μm^2)	100	-	100	-	4200	-	400	-	64	-
T_C (mK)	106	-	301.5	-	89.5	-	470	-	279.8	-
Outputs										
C ($\frac{fJ}{K}$)	0.35	0.36	n.p.	1.25	900	-	4.7	4.3	n.p.	0.3
G ($\frac{pW}{K}$)	44	44	n.p.	1589	117	117.8	110	-	n.p.	246.6
τ_{eff} (μs)	3.8	4.1	0.186	0.187	260	260.4	2.8	2.4	0.155	0.150
ΔE (eV)	0.11	0.11	0.26	0.26	2.5	2.3	0.52	0.52	0.21	0.21

This table compare the results of the simulations with the data taken from literature for five TESs. The acronyms "n.p." stands for "not present" meaning that data are not reported in the paper and the symbol "-" means that the literature value was used as input in the simulation.

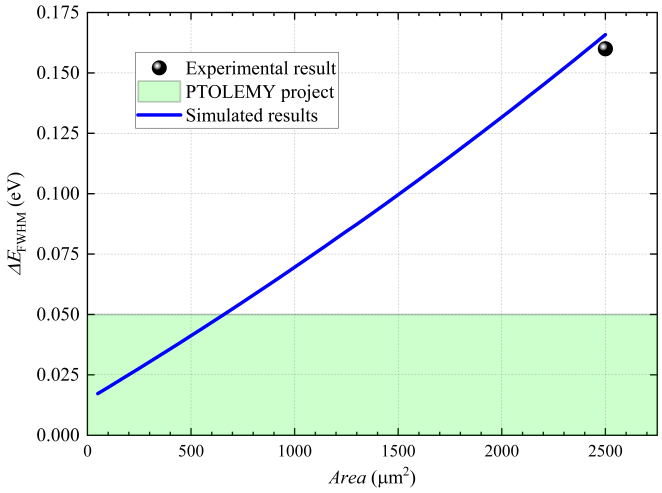

Fig. 3. The graph shows ΔE_{FWHM} measured for a 2500 μm^2 Ti/Au TES and expected ΔE_{FWHM} simulated with the software, in both cases $T_C = 52$ mK. Energy resolution better than 0.05 eV should be achieved for an equivalent TES with an active area below 650 μm^2.

Ti/Au TESs. The volume and the critical temperature are the two properties we are playing with to achieve the project goal, in fact, a small volume and a low T_C should guarantee an excellent energy resolution. However, we also aim to maximise the active area and optimize the T_C for the experimental system in which the detector will be used. For a Ti/Au bilayer the minimum Ti layer thickness that we are able to achieve preserving the superconductive properties is 12 nm. The minimum target value of T_C suitable for our system is between 50-60 mK. Considering these two constraints we studied the trend of T_C with respect to Au layer thickness with our program. From the simulation we apprehended that the superconductive transition of a Ti/Au bilayer with 12 nm and 30 nm thickness, respectively, is 58 mK. We fabricated and characterized a Ti/Au TES with an active area of 2500 μm^2 and the bilayer thicknesses reported above. The critical temperature resulted to be 52 mK, the thermal conductance 50 pW/K and the capacitance 2.5 fJ/K. With a bath temperature of 30 mK and a working point at 12 % of R_N, we measured an energy resolution of 0.16 eV for photons with 0.8 eV energy. We also measured $\alpha_I = 20$, $\beta_I = 5$ and $\tau_{eff} = 47$ μs. The complete characterization allowed us to replicate these results in our program and moreover simulate the energy resolution of an equivalent TES for different active areas. The graph in Fig. 3 shows the obtained experimental result and the results from the simulation. The target set by the PTOLEMY project is represented by the green area, according to the simulation, a TES with an area below 650 μm^2 should satisfy this requirement.

V. CONCLUSIONS

We have developed a simulation program that is a useful tool to predict and simulate the behaviour of rectangular TESs. The software has been tested through a comparison between literature and simulated results. We were able to simulate TESs performance in a broad range of applications, from optical to x-ray detection. The comparisons between the effective thermal time constants show an agreement within 16 %. The energy resolution, in case of optical TESs, matched with the experimental data while, for x-rays the agreement is within 8 %. The program is an effective tool that we are applying to the design phase of particle detection experiments. For PTOLEMY project, our simulation program was exploited to design the thicknesses required for the desired T_C and then to find the maximum area of the TES that could satisfy the project requirement. The program calculates TESs performances, whose agreement with the experimental data improves all the more devices parameters are known.
We provide a free access to the software as web application at url https://tes.inrim.it/ .

REFERENCES

[1] L. Lolli, E. Taralli, and M. Rajteri, "Ti/Au TES to discriminate single photons," *Journal of Low Temperature Physics*, vol. 167, no. 5, pp. 803–808, 2012.

[2] A. Giachero, B. Alpert, D. T. Becker, D. A. Bennett, M. Borghesi, M. De Gerone, M. Faverzani, M. Fedkevych, E. Ferri, G. Gallucci *et al.*, "Progress in the development of TES microcalorimeter detectors suitable for neutrino mass measurement," *IEEE Transactions on Applied Superconductivity*, vol. 31, no. 5, pp. 1–5, 2021.

[3] D. Fukuda, "Single-Photon Measurement Techniques with a Superconducting Transition Edge Sensor," *IEICE Transactions on Electronics*, vol. 102, no. 3, pp. 230–234, 2019.

[4] L. Lolli, E. Taralli, C. Portesi, E. Monticone, and M. Rajteri, "High intrinsic energy resolution photon number resolving detectors," *Applied Physics Letters*, vol. 103, no. 4, p. 041107, 2013.

[5] M. Rajteri, M. Biasotti, M. Faverzani, E. Ferri, R. Filippo, F. Gatti, A. Giachero, E. Monticone, A. Nucciotti, and A. Puiu, "TES Microcalorimeters for PTOLEMY," *Journal of Low Temperature Physics*, vol. 199, no. 1, pp. 138–142, 2020.

[6] S. Zhao, D. J. Goldie, C. N. Thomas, and S. Withington, "Calculation and measurement of critical temperature in thin superconducting multilayers," *Superconductor Science and Technology*, vol. 31, no. 10, p. 105004, 2018.

[7] R. Boucher, T. May, T. Wagner, V. Zakosarenko, S. Anders, and H. Mayer, "Structural and electrical properties of AuPd/Mo bilayer films for transition edge sensors," *Superconductor Science and Technology*, vol. 19, no. 1, p. 138, 2005.

[8] K. Irwin and G. Hilton, "Transition-Edge Sensors," in *Cryogenic Particle Detection*, C. Enss, Ed. Berlin, Heidelberg: Springer Berlin Heidelberg, 2005, pp. 63–150.

[9] J. C. Mather, "Bolometer noise: nonequilibrium theory," *Appl. Opt.*, vol. 21, no. 6, pp. 1125–1129, 1982.

[10] J. M. Martinis, G. C. Hilton, K. D. Irwin, and D. A. Wollman, "Calculation of Tc in a normal-superconductor bilayer using the microscopic-based Usadel theory," *Nuclear Instruments and Methods in Physics Research Section A: Accelerators, Spectrometers, Detectors and Associated Equipment*, vol. 444, no. 1-2, pp. 23–27, 2000.

[11] J. N. Ullom and D. A. Bennett, "Review of superconducting transition-edge sensors for x-ray and gamma-ray spectroscopy," *Superconductor Science and Technology*, vol. 28, no. 8, p. 084003, 2015.

[12] D. A. Bennett, D. S. Swetz, R. D. Horansky, D. R. Schmidt, and J. N. Ullom, "A two-fluid model for the transition shape in transition-edge sensors," *Journal of Low Temperature Physics*, vol. 167, pp. 102–107, 2012.

[13] J. E. Sadleir, S. J. Smith, S. R. Bandler, J. A. Chervenak, and J. R. Clem, "Longitudinal proximity effects in superconducting transition-edge sensors." *Physical review letters*, vol. 104 4, p. 047003, 2010.

[14] A. Kozorezov, A. A. Golubov, D. Martin, P. de Korte, M. A. Lindeman, R. Hijmering, J. van der Kuur, H. Hoevers, L. Gottardi, M. Y. Kupriyanov *et al.*, "Modelling the resistive state in a transition edge sensor," *Applied physics letters*, vol. 99, no. 6, p. 063503, 2011.

[15] F. Giazotto, T. T. Heikkilä, A. Luukanen, A. M. Savin, and J. P. Pekola, "Opportunities for mesoscopics in thermometry and refrigeration: Physics and applications," *Rev. Mod. Phys.*, vol. 78, pp. 217–274, Mar 2006.

[16] K. Irwin, "An application of electrothermal feedback for high resolution cryogenic particle detection," *Applied Physics Letters*, vol. 66, no. 15, pp. 1998–2000, 1995.

[17] G. Ventura and L. Risegari, "Properties of Solids at Low Temperature," in *The art of cryogenics: low-temperature experimental techniques*. Elsevier, 2010, pp. 55–84.

[18] E. F. Feliciano, "Theory and development of position-sensitive quantum calorimeters," PhD dissertation, Stanford University, 2001.

[19] K. M. Morgan, C. G. Pappas, D. A. Bennett, J. D. Gard, J. P. Hays-Wehle, G. C. Hilton, C. D. Reintsema, D. R. Schmidt, J. N. Ullom, and D. S. Swetz, "Dependence of transition width on current and critical current in transition-edge sensors," *Applied Physics Letters*, vol. 110, no. 21, p. 212602, 2017.

[20] A. Golubov, M. Kupriyanov, and E. Il'ichev, "The current-phase relation in Josephson junctions," *Reviews of Modern Physics*, vol. 76, pp. 411–469, 2004.

[21] Y. Geng, P.-Z. Li, J.-Q. Zhong, W. Zhang, Z. Wang, W. Miao, Y. Ren, and S.-C. Shi, "Temperature and current sensitivity extraction of optical superconducting transition-edge sensors based on a two-fluid model," *Chinese Physics B*, 2021.

[22] L. Lolli, E. Taralli, M. Rajteri, T. Numata, and D. Fukuda, "Characterization of optical fast transition-edge sensors with optimized fiber coupling," *IEEE transactions on applied superconductivity*, vol. 23, no. 3, pp. 2 100 904–2 100 904, 2013.

[23] E. Taralli, M. D'Andrea, L. Gottardi, K. Nagayoshi, M. Ridder, M. De Wit, D. Vaccaro, H. Akamatsu, M. Bruijn, and J. Gao, "Performance and uniformity of a kilo-pixel array of Ti/Au transition-edge sensor microcalorimeters," *Review of Scientific Instruments*, vol. 92, no. 2, p. 023101, 2021.

[24] R. Kobayashi, K. Hattori, S. Inoue, and D. Fukuda, "Development of a Fast Response Titanium-Gold Bilayer Optical TES With an Optical Fiber Self-Alignment Structure," *IEEE Transactions on Applied Superconductivity*, vol. 29, no. 5, pp. 1–5, 2019.